Indian Journal of Chemical Technology
Vol. 32, September 2025, pp. 593-604
DOI: 10.56042/ijct.v32i5.17493

Cattaneo-Christov heat flow analysis of hydromagnetic micropolar nanofluid over a chemically activated permeable stretching sheet

M. Vinodkumar Reddy[1], M. Ajithkumar[2], G. Sucharitha[3]* & P. Lakshminarayana[3]

[1]Department of Mathematics & Statistics, School of Applied Science & Humanities, Vignan's Foundation for Science, Technology & Research, Deshmukhi, Hyderabad-508284, India

[2]Department of Mathematics, Amrita School of Engineering, Amrita Vishwa Vidyapeetham, Chennai, India

[3]Department of Mathematics, School of Advanced Sciences, Vellore Institute of Technology, Vellore-632014, India

*E-mail: sarithagorintla@gmail.com

Received 27 February 2025; accepted 16 May 2025

Several engineering and technological processes, such as air conditioning, machinery power collectors, food processing, refrigeration, and heat exchangers, need deep investigation of energy and mass transfer in various conditions. As a result, in this paper, we analyze the radiative flow of a hydromagnetic micropolar nanofluid with activation energy and chemical reaction using the Cattaneo-Christov energy flux model over an expanding porous sheet. Further, the consequences of suction, energy generation, and convective boundary conditions were also examined. Boundary layer approximation is utilized to obtain the primary partial differential equations of the model and reduced to nonlinear ordinary differential equations, using the appropriate transformations, the model equations are formulated for numerical simulation and further analysis. Using the inbuilt BVP5C function available in MATLAB, the numerical solutions for the coupled system of the nonlinear ordinary differential equations are obtained. Further, graphical and tabular representations are used to analyze the impacts of several physical parameters on the concentration, velocity, temperature, and microrotation fields. The outcomes reveal that the velocity and microrotation of the micropolar liquid movement are improved by increasing the magnetic and material parameters. An increase in the concentration Grashof number, thermal relaxation parameter, and temperature Grashof number leads to a reduction in the temperature distribution within the thermal boundary layer. Furthermore, the mass transfer rate is directly proportional to the thermophoresis and chemical reaction parameters.

Keywords: Activation energy, Cattaneo-Christov model, Convective boundary conditions, Micropolar nanofluid, Nanofluid, Porous medium, Thermal radiation

Introduction

Several essential fluid flows in many industrial processes include boundary-layer activity over a continuously moving solid surface. These processes entail the extrusion of materials and the transfer of heat-treated components between a feed roll and a winding roll among numerous additional methods. In addition, non-Newtonian micropolar fluids exhibit unique rheological characteristics, making them suitable for a wide range of scientific and engineering applications, such as liquid crystals, polymeric suspensions, and biological fluids like blood. Due to their intrinsic microstructure and the ability to account for microrotational effects, these fluids fall under a broad classification that continues to inspire extensive research in fluid mechanics, biomedical engineering, and advanced material sciences. Given this, Hayat *et al.*[1] analyzed the mixed convective movement of a non-Newtonian micropolar liquid past a non-linear expanding surface. The time-dependent boundary layer movement of a radiative micropolar liquid past a permeable stretching surface through the utilization of the homotopy analysis technique was investigated by Hussain *et al.*[2]. Hsiao[3] used a finite difference approach to the magnetohydrodynamic transport of dissipative micropolar nanoliquid towards a stretchable sheet with convective energy transmission. Amjad *et al.*[4] performed the numerical simulation of Casson micropolar nano-liquid transport past an elongating sheet. Furthermore, recent investigations on the boundary layer flow of non-Newtonian fluids are presented in earlier reported articles[5-11].

In recognition of their superior thermodynamic features, nanofluids have garnered considerable interest in recent years. According to experimental research, a variety of aspects, such as the base fluid substance, size, temperature, shape, volume fraction, and composition of the particles, affect the thermal

stability of nanofluids. Considerable attention has been paid to electrically conducting nano-liquid flows, which react to the application of magnetic fields. The influence of energy source/sink and variable liquid properties on the hydromagnetic motion of dissipative fluid over a porous surface was analyzed by Dessie and Kishan[12]. Mabood *et al.*[13] examined the dissipative laminar flow of magneto water-based nano liquid past a nonlinear expanding surface. Additionally, they revealed that the temperature distribution is an elevating function of the Hartman number. Mishra *et al.*[14] presented the thermal flow of MHD convective homogeneous-heterogeneous reactions with micropolar nanofluid over a sheet. The influence of partial slip and convective boundaries on the MHD flow of micropolar liquid with Joule heating and micro-rotation effects was explored by Ramzan *et al.*[15]. Patel and Singh[16] addressed the convective hydromagnetic transport of radiative micropolar liquid due to a nonlinear porous sheet with Joule dissipation. The outstanding studies on hydromagnetic boundary layer flow of nanofluids have been reported[17-21].

It is commonly recognized that when two items possess distinct temperatures, heat transfer can occur both within a single object and between the two objects.The process of heat transport has received significant attention and is traditionally described by Fourier's law of heat conduction.The parabolic expression resulting from Fourier's law of heat conduction implies an unphysical, instantaneous propagation of thermal disturbances throughout the medium. To overcome this theoretical limitation, Cattaneo[22] introduced a thermal relaxation time into Fourier's equation, resulting in a hyperbolic model that allows heat to propagate at a finite speed via energy waves. The sway of the Cattaneo-Christov energy model on the viscous fluid movement past a linear porous expanding surface was scrutinized by Nadeem and Muhammad[23]. Rehman *et al.*[24] described the consequences of heat source and radiative heat flux on MHD micropolar liquid across a stretchable sheet. The Cattaneo-Christov energy flux models of various heat transfer fluids have widespread application in engineering and industry[25-29].

It is vital to investigate the impact of energy creation and absorption in many physical situations, such as fluids experiencing exothermic or endothermic chemical processes. When heat generation or absorption occurs, the temperature distribution of fluid can change. This can have an impact on the pace at which particles settle in systems like semiconductor wafers, electronic circuits, and nuclear reactors. Although it is challenging to calculate internal production or retention of energy precisely, there are a few basic mathematical models that can describe its typical behaviour in many real-world scenarios. To recognize this, Bataller[30] studied the consequence of internal energy production on dissipative boundary layer movement of a second-grade liquid across a non-isothermal expanding surface. A steady hydromagnetic flow of radiative Newtonian nanofluid via an expanding sheet in the presence of buoyancy impacts was investigated by Rashidi *et al.*[31]. Reddy *et al.*[32] discussed the thermal and solutal transport in magneto radiative flow of non-Newtonian fluid with heat generation and radiation. Goud[33] addressed the hydromagnetic micropolar liquid transportowing to a stretched surface with heat generation and suction/injection. Ram *et al.*[34] explored the consequences of activation energy on the hydromagnetic flow of micropolar liquid over an extended surface. Azam[35] performed research on the axisymmetric transport of radiative Maxwell nano liquid by considering a non-Fourier heat flux model with activation energy. Furthermore, researchers[36-38] have delved into the investigation of heat transfer and activation energy with nanofluids.

The key objective of this investigation is to analyse the radiative flow of an incompressible hydromagnetic micropolar nanofluid and activation energy using the Cattaneo-Christov energy flux model on an expanding porous sheet while including the consequences of suction, energy generation, chemical reaction and convective boundary conditions. Boundary layer approximation is implemented to represent the primary governing equations of this investigation. Then, by employing the appropriate conversion, the models are rebuilt into nonlinear coupled ordinary differential equations. Using the inbuilt BVP5C function available in MATLAB, numerical solutions for this examination are established. Further, the graphical and tabular representations allow us to analyse the impacts of several relevant parameters on the fluid concentration, temperature, velocity, and micro-rotation fields. The outcomes reveal that the micro rotation and velocity in the micropolar fluid flow are improved by applying positive amounts of the material number and Hartman parameter. Boosting the values of the concentration Grash of parameter, thermal relaxation time parameter, and thermal Grashof number assists in a decrease in the thermal field.

Formulation of the problem

In the present study, we consider the effect of the Arrhenius activation energy on the hydromagnetic radiative flow of a micropolar nanofluid with the Cattaneo-Christov energy flux past a stretching sheet in a porous medium under convective boundary conditions. The Arrhenius activation energy is incorporated into the concentration equation to account for the temperature-dependent chemical reaction rates. This allows us to model the impact of varying temperatures on the reaction rate, which in turn influences the concentration distribution of the fluid, thereby affecting the overall heat and mass transfer behaviour in the system. Brownian motion, thermophoresis and heat generation are also considered to enhance the heat transfer.

It is considered that the sheet is stretched in the direction of x axis with velocity $u_w = bx$ (here $b$denotes the stretching constant), while the fluid is placed along y axis. Let (u, v) denote the components along the (x, y) path correspondingly. The magnetic field strength B_0 acts perpendicular to the flow. The system of physical flow model and geometry are exhibited in Fig. 1. Under these assumptions, the governing boundary layer equations can be written as[8,24] follows:

$$\frac{\partial u}{\partial x}+\frac{\partial v}{\partial y}=0 \qquad \text{... (1)}$$

$$u\frac{\partial u}{\partial x}+v\frac{\partial u}{\partial y}=\left(\frac{\mu+k}{\rho}\right)\frac{\partial^2 u}{\partial y^2}+\left(\frac{k}{\rho}\right)\frac{\partial N}{\partial y} - \frac{\sigma\beta_0^2 u}{\rho}-\frac{\mu}{\rho k_1}u + \mathrm{g}\beta_T(T-T_\infty) + \mathrm{g}\beta_C(C-C_\infty) \qquad \text{... (2)}$$

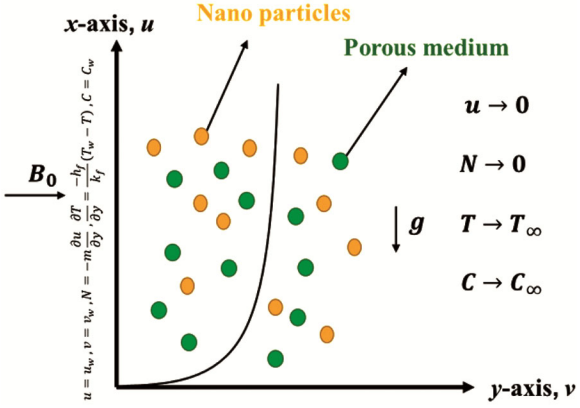

Fig. 1 — Physical model

$$\left(u\frac{\partial N}{\partial x}+v\frac{\partial N}{\partial y}\right)=\left(\frac{\gamma^*}{\rho j}\right)\frac{\partial^2 N}{\partial y^2} - \left(\frac{k}{\rho j}\right)\left(2N+\frac{\partial u}{\partial y}\right) \qquad \text{... (3)}$$

$$u\frac{\partial T}{\partial x}+v\frac{\partial T}{\partial y}=\alpha\frac{\partial^2 T}{\partial y^2}+\left(\frac{\mu+k}{\rho C_P}\right)\left(\frac{\partial u}{\partial y}\right)^2 + \tau\left(D_B\frac{\partial c}{\partial y}\frac{\partial T}{\partial y}+\frac{D_T}{T_\infty}\left(\frac{\partial T}{\partial y}\right)^2\right) - \frac{1}{\rho C_P}\frac{\partial q_r}{\partial y}+\frac{Q_o}{\rho C_P}(T-T_\infty) - \lambda\left[u\frac{\partial u}{\partial x}\frac{\partial T}{\partial x}+v\frac{\partial v}{\partial y}\frac{\partial T}{\partial y}+u\frac{\partial v}{\partial x}\frac{\partial T}{\partial y}+v\frac{\partial u}{\partial y}\frac{\partial T}{\partial x} + 2uv\frac{\partial^2 T}{\partial x\partial y}+u^2\frac{\partial^2 T}{\partial x^2}+v^2\frac{\partial^2 T}{\partial y^2}\right] \qquad \text{... (4)}$$

$$u\frac{\partial C}{\partial x}+v\frac{\partial C}{\partial y}=D_B\frac{\partial^2 C}{\partial y^2}+\frac{D_T}{T_\infty}\frac{\partial^2 T}{\partial y^2} - K_r{}^2(C-C_\infty)\left(\frac{T}{T_\infty}\right)^n exp\left(\frac{-E_a}{kT}\right). \qquad \text{... (5)}$$

The appropriate boundary conditions are:

$$u=u_w\,,v=v_w\,,N=-m\frac{\partial u}{\partial y}\,,\frac{\partial T}{\partial y} =\frac{-h_f}{k_f}(T_w-T)\,,C = C_w \;\; at\; y=0, \qquad \text{... (6)}$$

$$u\to 0, N\to 0, T\to T_\infty\,, C\to C_\infty \;\; as\; y\to\infty\,. \qquad \text{... (7)}$$

Introducing the similarity transformations as below:

$$u=bxf'(\eta)\,,v=-(b\vartheta)^{\frac{1}{2}}f(\eta)\,,N=bx\sqrt{\frac{b}{\vartheta}}\,,\eta =\sqrt{\frac{b}{\vartheta}}\,y\,, \theta(\eta)(T_w-T_\infty)=T-T_\infty\,,\varphi(\eta)(C_w-C_\infty) =C-C_\infty \qquad \text{... (8)}$$

and substituting Eq. (8) in Eqs. (2) - (7), we obtained the following non-dimensional equations:

$$(1+K)f'''-(K_P+M)f'+Kg'+f''f+\lambda_1\theta + \lambda_2\phi-f'^2=0, \qquad \text{... (9)}$$

$$\left(\frac{K}{2}+1\right)g''+g'f-gf'-(f''+2g)K=0, \quad \ldots (10)$$

$$Pr\left[-f'\theta' f\delta+Nb\varphi'\theta'+\theta' f+Ec(1+K)f''^{2}+\theta'^{2}Nt+Q\theta\right]+\left(-\delta Prf^{2}+(1+R)\right)\theta''=0, \quad \ldots (11)$$

$$\varphi''+Scf\varphi'+\frac{Nt}{Nb}\theta''-Sc\gamma exp\left(\frac{-E}{1+\theta\alpha_1}\right)(1+\theta\alpha_1)^{n}\varphi=0. \quad \ldots (12)$$

The corresponding boundary constraints are:

$$f(0)=s, f'(0)=1, g(0)=-mf''(0), \theta'(0)=-Bi\left(1-\theta(0)\right), \varphi(0)=1, \quad \ldots (13)$$

$$f'(\infty)=0, g(\infty)=0, \theta(\infty)=0, \varphi(\infty)=0, \quad \ldots (14)$$

Where

$$M=\frac{\sigma B_{\circ}^{2}}{\rho b},\ K_p=\frac{\upsilon}{bk_1},\ K=\frac{k}{\rho\upsilon},\ \lambda_1=\frac{g\beta_T\left(T_w-T_\infty\right)}{bu_w},$$
$$\lambda_2=\frac{g\beta_C\left(C_w-C_\infty\right)}{bu_w},\ \delta=b\lambda,\ R=\frac{16\sigma^{*}T_\infty^{3}}{3k^{*}k},\ Pr=\frac{\upsilon}{\alpha},$$
$$Q=\frac{Q_{\circ}}{\rho C_p b},\ Ec=\frac{u_w^{2}}{\left(T_w-T_\infty\right)C_p},$$
$$Nb=\frac{\tau D_B\left(C_w-C_\infty\right)}{\upsilon},\ Nt=\frac{\tau D_T\left(T_w-T_\infty\right)}{T_\infty\upsilon},$$
$$Sc=\frac{\upsilon}{D_B},\ \gamma=\frac{K_r^{2}}{b},\ E=\frac{E_a}{kT_\infty},\ S=-\frac{v_w}{\sqrt{b\upsilon}},\ Bi=\frac{h_f}{k}\sqrt{\frac{\upsilon}{b}}. \quad \ldots (15)$$

The friction factor, couple stress, Nusselt and Sherwood numbersare defined as follows:

$$C_f(Re)^{0.5}=2\left(1+K(1-m)\right)f''(0),\ C_S(Re)^{0.5}=\left(1+\frac{K}{2}\right)g'(0),$$
$$Nu(Re)^{-0.5}=-(1+R)\theta'(0),\ Sh(Re)^{-0.5}=-\varphi'(0) \quad \ldots (16)$$

Where $Re=\frac{bx^{2}}{\upsilon}$ is the local Reynolds parameter.

Solution of the problem

The obtained dimensionless Eqs (9) - (12) and the corresponding boundary constraints (13)-(14) are solved numerically by BVP5C inbuilt MATLAB tool. The consequent more complex ODEs are converted into the first-order ODEs by employing the following connections.$f_1=f, f_2=f', f_3=f''$, $f_4=g$, $f_5=g'$, $f_6=\theta$, $f_7=\theta'$ $f_8=\varphi$, $f_9=\varphi'$. Then the reduced equations are framed out in:

$$f_1'=f(2), \quad \ldots (17)$$

$$f_2'=f(3), \quad \ldots (18)$$

$$f_3'=\left(\frac{1}{(1+K)}\right)[(M+K_P)f_2-f_1f_3-K f_5-\lambda_1 f_6-\lambda_2 f_8+f_2f_2], \quad \ldots (19)$$

$$f_4'=f(5), \quad \ldots (20)$$

$$f_5'=\frac{1}{\left(1+\frac{K}{2}\right)}[f_2 f_4-f_1 f_5+K(2 f_4+f_3)], \quad \ldots (21)$$

$$f_6'=f(7), \quad \ldots (22)$$

$$f_7'=\frac{1}{[(1+R)-Pr\delta f_1f_1]}(Pr[\delta f_1f_2 f_7-f_1 f_7-Q f_6-Nb f_7 f_9-Nt f_7 f_7-(1+K)Ecf_3f_3]), \quad \ldots (23)$$

$$f_8'=f(9), \quad \ldots (24)$$

$$f_9'=-\frac{Nt}{Nb}\left[\frac{1}{[(1+R)-Pr\delta f_1f_1]}(Pr[\delta f_1f_2 f_7-f_1 f_7-Q f_6-Nb f_7 f_9-Nt f_7 f_7-(1+K)Ecf_3f_3])\right]-Scf_1f_9+Sc\gamma(1+\alpha_1 f_6)^{n}exp\left(\frac{-E}{1+\alpha_1 f_6}\right)f_8. \quad \ldots (25)$$

The appropriate boundary conditions are

$$f_1=S, f_2=1, f_4=-mf_3, f_7=-Bi(1-f_6), f_8=1\ at\ \eta=0, \quad \ldots (26)$$

$$f_2=0, f_4=0, f_6=0, , f_8=0\ as\ \eta\to\infty. \quad \ldots (27)$$

Discussion

The altered controlling Eqs (9) - (12) and the related boundary constraints (13) and (14), which

show significant coupling and non-linearity, are very complex, hence in this case, we have chosen a numerical solution. The impact of several variables on the movement of a micropolar nano liquid across an expanded surface with a porous media, including heat production, activation energy, suction, viscous dissipation, thermal radiation, and magnetic field, is addressed by this numerical solution**.** The numerical solutions for fluid velocity $f'(\eta)$, micro rotation $g(\eta)$, thermal field $\theta(\eta)$, concentration profile $\phi(\eta)$, skin friction, mass, and heat transmission rates are computed for a range of effective flow parameters.These parameters includethemagnetic parameter M, micropolar fluid parameter K, thermophoresis parameter Nt, porosity parameter K_p, energy creation parameter Q, Brownian movement parameter Nb, Schmidt number Sc, chemical reaction parameter γ, thermal Biot number Bi, thermal Grashof number λ_1, Eckert number Ec, concentration Grashof number λ_2,activation energy parameter E, thermal relaxation time parameter δ, radiation parameter R, and boundary parameter m.

The behaviour of the magnetic parameter M on the liquid velocity distribution is shown in Fig. 2a. The graph demonstrates that as the magnetic number M elevates in magnitude, the $f'(\eta)$ decreases. Furthermore, an increase in the Lorentz force associated with the magnetic field leads to greater resistance within the flow field. Figs 2b and 2c demonstrate the influence of the magnetic number M on microrotation and thermal profiles. Analysing these figures reveals that elevated magnetic number values amplify both the temperature $\theta(\eta)$ and micro rotation $g(\eta)$ profiles. Additionally, the thermal boundary layer thickness experiences an augmentation under the influence of higher magnetic numbers. The influence of the micropolar fluid parameter K on micro rotation $g(\eta)$ is seen in Fig. 3, where there is a noticeable reduction in micro rotation. A pictogram of the velocity $f'(\eta)$ and microrotation $g(\eta)$ distribution for various amounts of the permeability parameter K_p while holding the remaining parameters constant is shown in Fig. 4 Physically, an increase in the porosity of the porous medium leads to a decrease in velocity and an enhancement in micro-rotation profiles. The effect of the temperature Grashof parameter λ_1 on the thermal profile is depicted in Fig. 5. It is perceived from this illustration that the fluid velocity $f'(\eta)$ enhances for greater amounts of λ_1. Further, Fig. 6 illustrates an enhancement in the micro rotation distribution $g(\eta)$ as the surface boundary number m increases. The

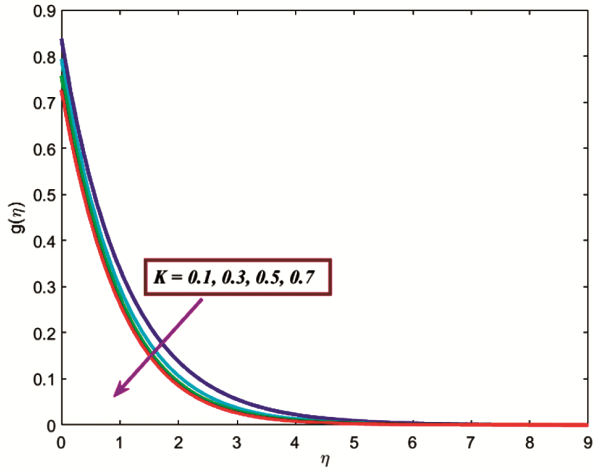

Fig. 3 — Behaviour of Kon micro rotation

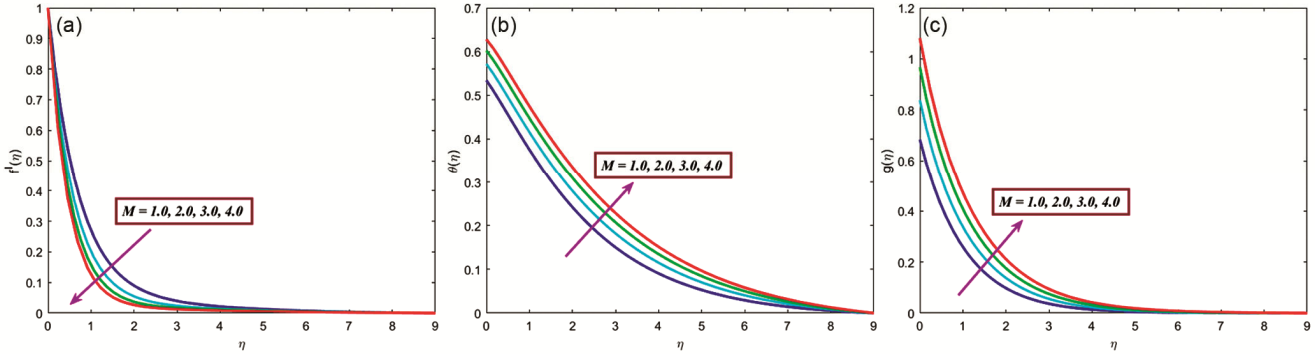

Fig. 2 — Behaviour of Mon (a) velocity, (b) temperature and (c) micro rotation

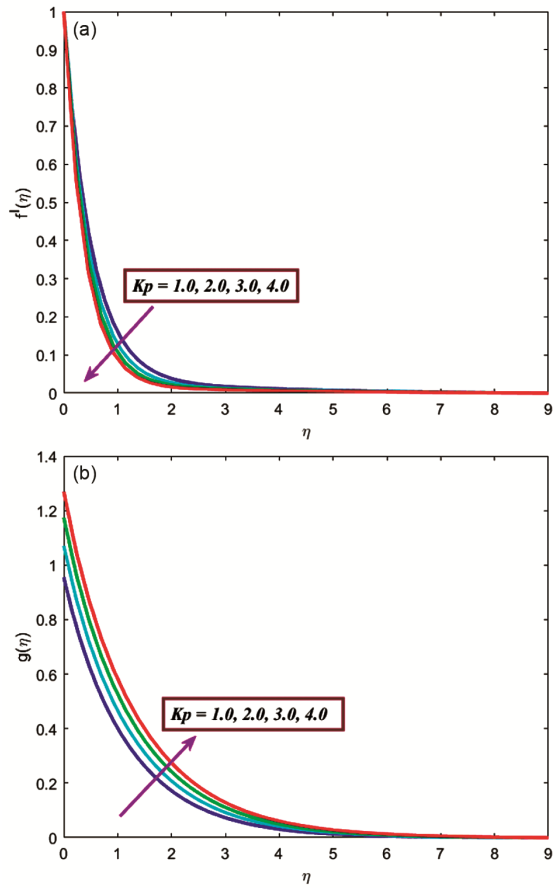

Fig. 4 — Behaviour of Kp on (a) velocity, (b) micro rotation

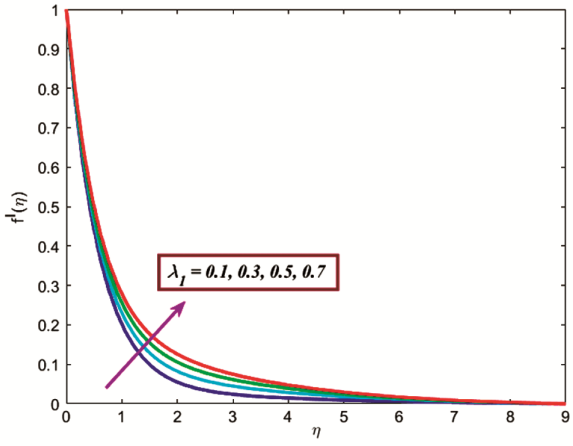

Fig. 5 — Behaviour of λ_1 on velocity

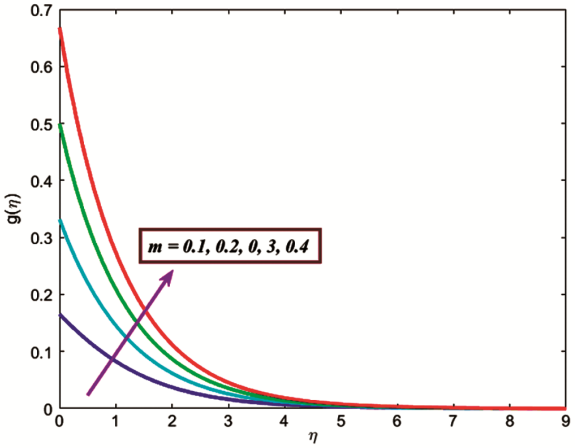

Fig. 6 — Behaviour of m on micro rotation

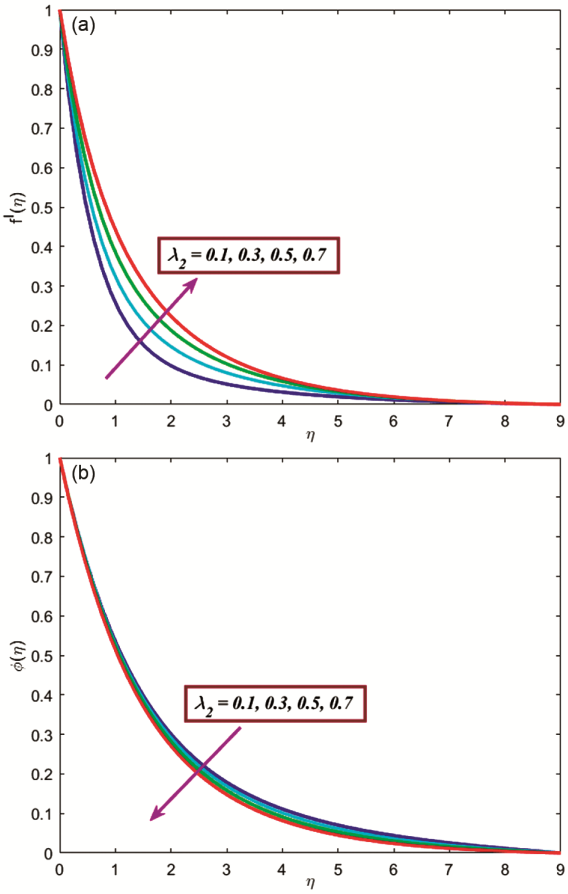

Fig. 7 — Behaviour of λ_2 on (a) velocity and (b) concentration

impacts of the concentration Grashof number λ_2 on velocity, and concentration profiles are depicted in Figs 7a and 7b, respectively. It is noted that an increase in the relevant parameter leads to a reduction in concentration field.However, an increase in the velocity distribution $f'(\eta)$ is noted under the influence of the same parameter. The consequences of the radiation parameter R and Eckert parameter Ec on the thermal distribution of the micropolar nanofluid are portrayed in Figs 8a and 8b. Due to the higher values of Ec and R, the temperature profile $\theta(\eta)$ is increased along with its boundary thickness.

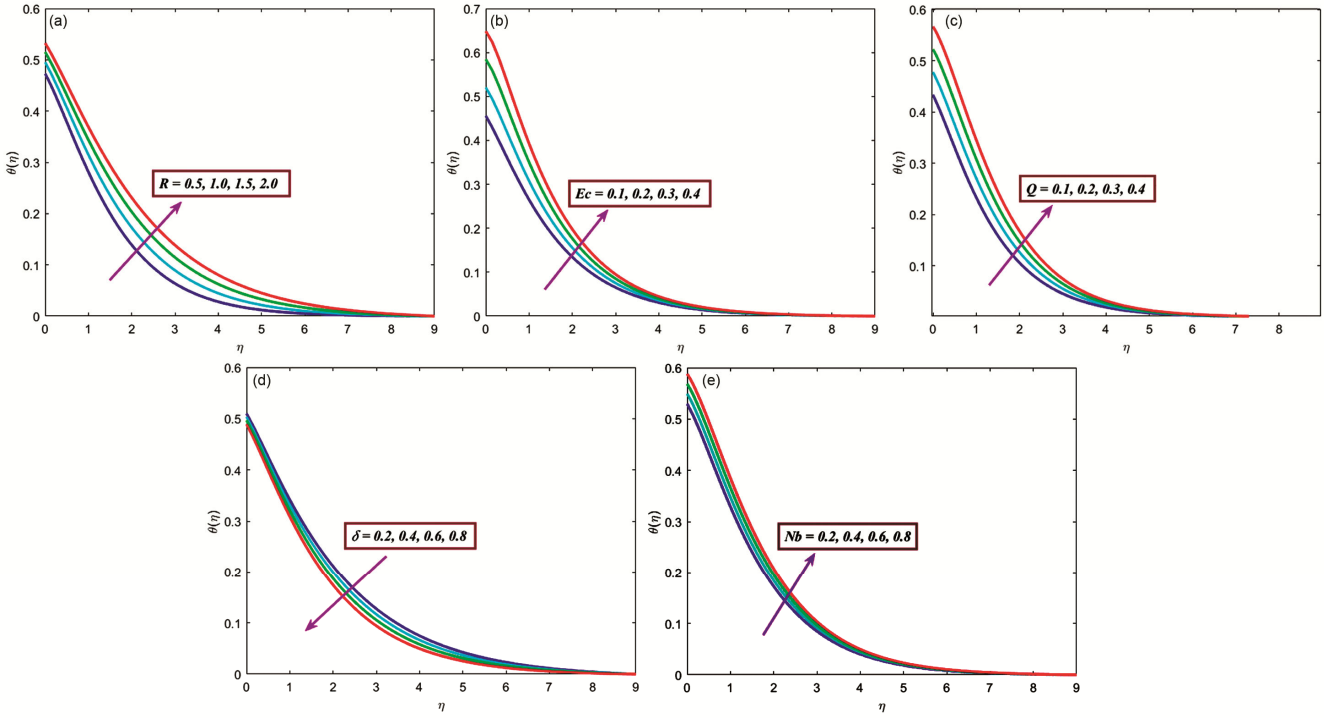

Fig. 8 — Behaviour of (a) R, (b) Ec, (c) Q, (d) δ and (e) Nb on temperature

Physically, the thermal energy in the fluid is retained at higher levels of Ec. The temperature profile $\theta(\eta)$ is ventually enhanced owing to friction forces. Fig. 8c outlines the sway of energy generation Q on the thermal field $\theta(\eta)$. The thermal boundary layer increases in thickness as the heat generation parameter value rises. Generally, the higher heat source generates additional thermal energy on the fluid flow which leads to a higher thermal field $\theta(\eta)$. The thermal boundary layer becomes thinner as the thermal relaxation time parameter δ increases as seen in Fig. 8d, demonstrating that the thermal relaxation parameter is causing the temperature field $\theta(\eta)$ to drop. In other words, it impacts the strength of heat transmission. As a result, the opposite delayed effects of δ on the temperature field occur further away from the surface. Fig. 8e illustrates how the thermal profile $\theta(\eta)$ is influenced by variations in the Brownian movement parameter Nb. The depiction highlights the significant impact that changes in the Brownian motion parameter can have on this profile. The figure demonstrates that an elevation in the Brownian movement parameter leads to a corresponding rise in the temperature profile $\theta(\eta)$. The relationship between the thermophoresis effect Nt and concentration field $\phi(\eta)$ is visually represented in Fig. 9a, providing a clear insight into the influence of this parameter on the system. It is evident that with an increase in the values of the thermophoresis parameter, both the concentration profile $\phi(\eta)$ of the micropolar nanofluid and the solute boundary layer thickness of the sheet experience a decline. The consequence of the activated energy parameter E on the fluid concentration $\phi(\eta)$ is depicted in Fig. 9b. Here, noted that higher E improves the concentration distribution. The concentration distribution $\phi(\eta)$ as a function of the Schmidt parameter Sc and the chemical reaction γ is depicted in Fig. 9c and Fig. 9d, respectively. It is identified that the parameter Sc controls the concentration field $\phi(\eta)$ of the micropolar nanofluid. In the same manner, the higher chemical reaction brings down the concentration field. This is because an increasing value of the rate of chemical reaction γ leads to the consumption of a greater number of chemically reacting species. Figs 10(a–b) and 11(a–b) illustrate the variations in

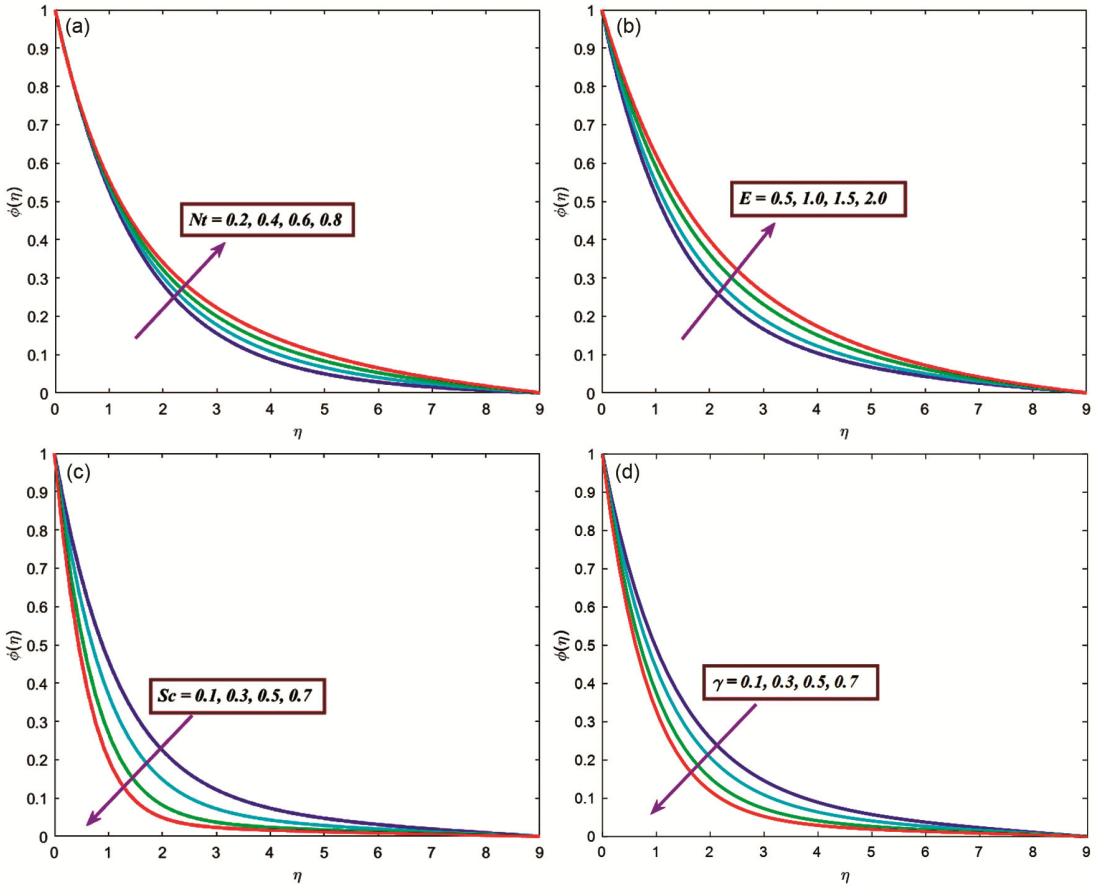

Fig. 9 — Behaviour of (a) Nt, (b) E, (c) Sc and (d) γ on concentration

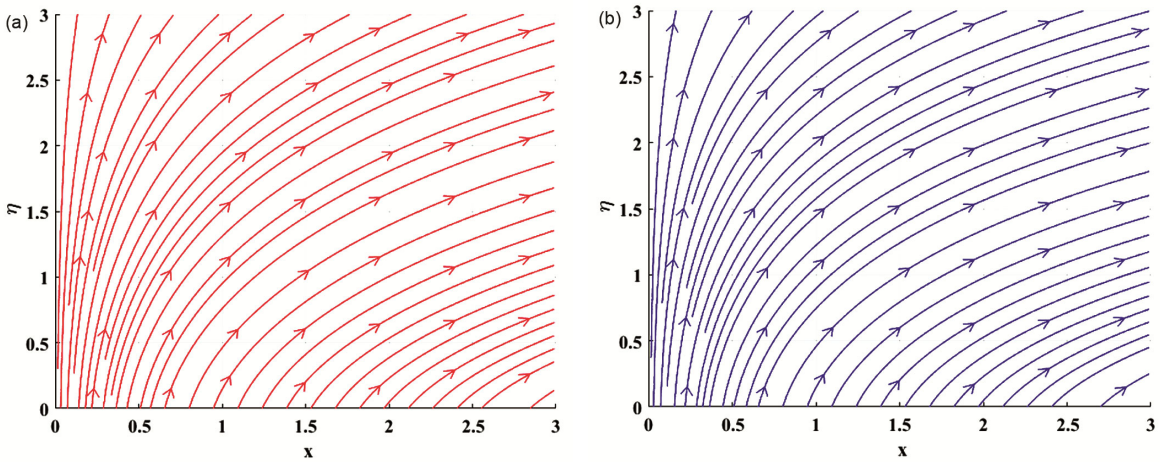

Fig. 10 — Streamlines for (a) M = 1 and (b) M = 1.5

streamlines and contour plots with increasing values of the magnetic parameter M.

Tables 1-3 demonstrate the behaviour of the friction factor $C_f\left(Re_x\right)^{0.5}$, Sherwood number $Sh\left(Re_x\right)^{-0.5}$, and Nusselt number $Nu\left(Re_x\right)^{-0.5}$ for numerous levels of pertinent flow parameters. From Table 1, it is observed that $C_f\left(Re_x\right)^{1/2}$ increases by increasing amounts of λ_1, λ_2, and m. However, the opposite trend is identified for M, K_p, and K. Table 2

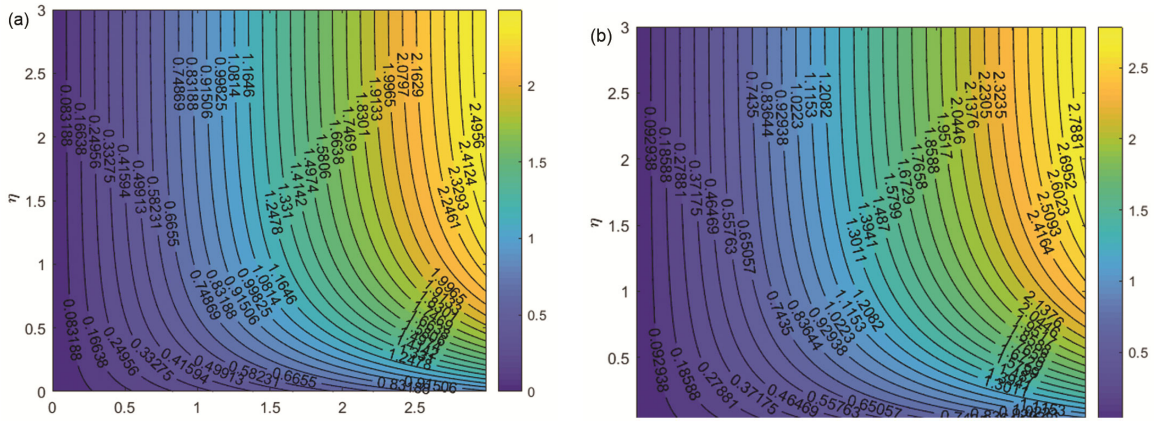

Fig. 11 — Contour plots for (a) $M = 1$; (b) $M = 1.5$

Table 1 — Variations in skin friction, couple stress for various parameter values

M	K_P	K	λ_1	λ_2	S	m	$C_f(Re_x)^{\frac{1}{2}}$	$C_s(Re_x)^{\frac{1}{2}}$
1.0							-2.870323	-0.708743
2.0							-3.518163	-0.833037
3.0							-4.062427	-0.929999
	1.0						-4.011283	-0.921148
	2.0						-4.495049	-1.003207
	3.0						-4.930694	-1.074077
		0.1					-3.518163	-0.833037
		0.3					-3.650474	-0.885405
		0.5					-3.786873	-0.917649
			0.1				-3.518163	-0.833037
			0.3				-3.379249	-0.816145
			0.5				-3.251448	-0.797926
				0.1			-3.518163	-0.833037
				0.3			-3.344715	-0.807267
				0.5			-3.172397	-0.778888
					0.1		-3.518163	-0.833037
					0.2		-3.623291	-0.907056
					0.3		-3.731437	-0.987082
						0.1	-3.606906	-0.108055
						0.2	-3.584964	-0.288100
						0.3	-3.562860	-0.468945

depicts that the rate of heat transfer is an increasing function of R, δ, Bi, and S, whereas the opposite behaviour for M, Nb, Nt, and Ec is observed. Table 3 shows an enhancing trend for Nt, S and γ, however, the opposite behaviour is discovered for Nb, E, and Bi.

In Table 4, the Nusselt number is compared against the results of Rehman et al.[24] for different values of the Brownian motion parameter Nb, under the conditions $K_p = \delta = Ec = E = 0$. The excellent agreement between the two studies serves as a robust validation of the present computational model. The matching of values up to the sixth decimal place highlights the adequacy of the validation. This high level of agreement is attributed to the fact that both the present study and Rehman et al.[24] employed the same numerical solution methodology, specifically the BVP5C solver in MATLAB. This consistency in the computational approach ensures that any discrepancies due to numerical implementation are minimized, leading to near-identical results under identical physical conditions.

It is also important to note that the validation is justified based on the alignment of physical assumptions. By setting the parameters $K_p = \delta = Ec = E = 0$, the present study deliberately removes the additional effects considered beyond those in the

Table 2 — Variations in rate of heat transfer for various parameter values

M	R	Nb	Nt	δ	Q	Ec	S	Bi	$Nu(Re_x)^{-\frac{1}{2}}$
1.0									0.227981
2.0									0.196105
3.0									0.170501
	0.5								0.155379
	1.0								0.196105
	1.5								0.236129
		0.2							0.200542
		0.4							0.191870
		0.6							0.183614
			0.2						0.197609
			0.4						0.194587
			0.6						0.191510
				0.1					0.195987
				0.2					0.196105
				0.3					0.196244
					0.1				0.196105
					0.2				0.164604
					0.3				0.133425
						0.1			0.196055
						0.2			0.162189
						0.3			0.128525
							0.1		0.196105
							0.2		0.211922
							0.3		0.227376
								0.1	0.104093
								0.3	0.196105
								0.5	0.238170

Table 3 — Variations in rate of mass transfer for various parameter values

Nb	Nt	γ	E	S	Bi	$Sh(Re_x)^{-\frac{1}{2}}$
0.2						0.658067
0.4						0.646082
0.6						0.642660
	0.2					0.641020
	0.4					0.659396
	0.6					0.679844
		0.1				0.403413
		0.3				0.543944
		0.5				0.649950
			0.5			0.584044
			1.0			0.496532
			1.5			0.432867
				0.1		0.649950
				0.2		0.667654
				0.3		0.686101
					0.1	0.652180
					0.3	0.649950
					0.5	0.649197

reference study. Under these specific conditions, the governing equations and boundary conditions of the present model coincide with those used by Rehman et al.[24]. As a result, the close match between the datasets confirms the correctness of the present study and demonstrates that any further deviations in

Table 4 — Validation of $Nu(Re_x)^{-0.5}$ for *Nb* when $K_p = \delta = Ec = E = 0$

Nb	Rehman et al.[24]	Present study
0.2	0.273023	0.273023
0.4	0.265590	0.265590
0.6	0.258207	0.258207

extended simulations stem from the influence of the additional physical effects introduced in our formulation.

Conclusion

In this study, we analyzed energy and mass transport in a 2D hydromagnetic non-Newtonian micropolar nano-liquid. The impacts of the Brownian motion and the thermophoresis by using the Cattaneo-Christov model are investigated. The study also considered the impacts of energy source, viscous heating and activating energy. The numerical solution for the governing equations allows for the determination of flow as heat and mass transfer characteristics over a wide range of parametric values. As the micropolar fluid parameter, the porosity parameter, and the magnetic parameter increase, there is a decrease in velocity distributions. The micro rotation profile exhibits an increase due to an increase in the porosity parameter. Increase in the values of the thermal relaxation parameter, the concentration Grashof number and the thermal Grashof number lead to a decrease in the temperature profile. The Nusselt number distribution declines with the elevation of the Brownian movement, thermophoresis parameter and the Eckert number but a reverse trend is observed because of increased radiation, the Biot number and the suction parameter. The Sherwood number is directly proportional to the thermophoresis parameter and the chemical reaction parameter.

Conflict of interest

The authors declare no conflict of interest.

References

1 Hayat T, Abbas Z & Javed T, Mixed convection flow of a micropolar fluid over a non-linearly stretching sheet, *Phys Lett A*, 372 (2008) 637.

2 Hussain M, Ashraf M, Nadeem S & Khan M, Radiation effects on the thermal boundary layer flow of a micropolar fluid towards a permeable stretching sheet, *J Frank Inst*, 350 (2013) 194.

3 Kai-Long H, Micropolar nanofluid flow with MHD and viscous dissipation effects towards a stretching sheet with multimedia feature, *Int J Heat Mass Transf*, 112 (2017) 983.

4 Amjad M, Zehra I, Nadeem S & Abbas N, Thermal analysis of Casson micropolar nanofluid flow over a permeable curved stretching surface under the stagnation region, *J Therm Anal Calorim*, 143 (2021) 2485.

5 Rashad A M, Nafe M A & Eisa D A, Heat generation and thermal radiation impacts on flow of magnetic Eyring–Powell hybrid nanofluid in a porous medium, *Arab J Sci Eng*, 48 (2023) 939.

6 Sumithra A, Sivaraj R, Benazir A J & Makinde O D, Nonlinear thermal radiation and activation energy effects on bioconvective flow of Eyring-powell fluid, *Comput Therm Sci Int J*, 13 (2021) 85.

7 Jasmine B A, Sivaraj R & Rashidi M M, Comparison between Casson fluid flow in the presence of heat and mass transfer from a vertical cone and flat plate, *J Heat Transf*, 138 (2016) 112005.

8 Saidulu B & Reddy K S, Evaluation of combined heat and mass transfer in hydromagnetic micropolar flow along a stretching sheet when viscous dissipation and chemical reaction is present, *Partial Differ Equ Appl Math*, 7 (2023) 100467.

9 Boroumand A M, Morra G & Mora P, Extracting fundamental parameters of 2D natural thermal convection using convolutional neural networks, *J Appl Phys*, 135 (2024) 144702.

10 Yi-Xia L, Alshbool M H, Yu-Pei L, Khan I, Khan M R & Issakhov A, Heat and mass transfer in MHD Williamson nanofluid flow over an exponentially porous stretching surface, *Case Stud Therm Eng*, 26 (2021) 100975.

11 Safdar R, Jawad M, Hussain S, Imran M, Akgül A & Jamshed W, Thermal radiative mixed convection flow of MHD Maxwell nanofluid: Implementation of buongiorno's model, *Chin J Phys*, 77 (2022) 1465.

12 Dessie H & Kishan N, MHD effects on heat transfer over stretching sheet embedded in porous medium with variable viscosity, viscous dissipation and heat source/sink, *Ain Shams Eng J*, 5 (2014) 967.

13 Mabood F, Khan W A & Ismail A M, MHD boundary layer flow and heat transfer of nanofluids over a nonlinear stretching sheet: A numerical study, *J Magn Magn Mater*, 374 (2015) 569.

14 Mishra S R, Mathur P & Ali H M, Analysis of homogeneous–heterogeneous reactions in a micropolar nanofluid past a nonlinear stretching surface: Semi-analytical approach, *J Therm Anal Calorim*, 144 (2021) 2247.

15 Ramzan M, Farooq M, Hayat T & Chung J D, Radiative and Joule heating effects in the MHD flow of a micropolar fluid with partial slip and convective boundary condition, *J Mol Liq*, 221 (2016) 394.

16 Patel H R & Singh R, Thermophoresis, brownian motion and non-linear thermal radiation effects on mixed convection MHD micropolar fluid flow due to nonlinear stretched sheet in porous medium with viscous dissipation, joule heating and convective boundary condition, *Int Commun Heat Mass Transf*, 107 (2019) 68.

17 Gupta S S, Siva V M, Krishnan S, Sreeprasad T S, Singh P K, Pradeep T & Das S K, Thermal conductivity enhancement of nanofluids containing graphene nanosheets, *J Appl Phys*, 110 (2011) 084302.

18 Kausar M S, Hussanan A, Waqas M & Mamat M, Boundary layer flow of micropolar nanofluid towards a permeable stretching sheet in the presence of porous medium with thermal radiation and viscous dissipation, *Chin J Phys*, 78 (2022) 435.

19 Varatharaj K, Tamizharasi R, Sivaraj R & Vajravelu K, Simulation of MHD-Casson hybrid nanofluid dynamics over a permeable stretching sheet: Effects of heat transfer and thermal radiation, *J Therm Anal Calorim*, 149 (2024) 8693.

20 Reddy M V & Lakshminarayana P, Cross-diffusion and heat source effects on a three-dimensional MHD flow of Maxwell nanofluid over a stretching surface with chemical reaction, *Eur Phys J Spec Top*, 230 (2021) 1371.

21 Ramandevi B, Reddy J V R, Sugunamma V & Sandeep N, Combined influence of viscous dissipation and non-uniform heat source/sink on MHD non-Newtonian fluid flow with Cattaneo-Christov heat flux, *Alex Eng J*, 57 (2018) 1009.

22 Cattaneo C, Sulla conduzione del calore, *Atti Sem Mat Fis Univ Modena*, 3 (1948) 83.

23 Nadeem S & Muhammad N, Impact of stratification and Cattaneo-Christov heat flux in the flow saturated with porous medium, *J Mol Liq*, 224 (2016) 423.

24 Rehman S U, Mariam A, Ullah A, Asjad M I, Bajuri M Y, Pansera B A & Ahmadian A, Numerical computation of buoyancy and radiation effects on MHD micropolar nanofluid flow over a stretching/shrinking sheet with heat source, *Case Stud Therm Eng*, 25 (2021) 100867.

25 Salmi A, Madkhali H A, Ali B, Nawaz M, Alharbi S O & Alqahtani A S, Numerical study of heat and mass transfer enhancement in Prandtl fluid MHD flow using Cattaneo-Christov heat flux theory, *Case Stud Therm Eng*, 33 (2022) 101949.

26 Shah Z, Shafiq A, Rooman M, Alshehri M & Bonyah E, Darcy forchhemier prandtl-eyringnanofluid flow with variable heat transfer and entropy generation using Cattaneo-Christov heat flux model: Statistical approach, *Case Stud Therm Eng*, 49 (2023) 103376.

27 Saleem S, Awais M, Nadeem S, Sandeep N & Mustafa M T, Theoretical analysis of upper-convected Maxwell fluid flow with Cattaneo-Christov heat flux model, *Chin J Phys*, 55 (2017) 1615.

28 Waqas H, Fida M, Liu D, Manzoor U & Muhammad T, Numerical simulation of entropy generation for nanofluid with the consequences of thermal radiation and Cattaneo-Christov heat flux model, *Int Commun Heat Mass Transf*, 137 (2022) 106293.

29 Reddy M V & Lakshminarayana P, MHD radiative flow of Williamson nanofluid with Cattaneo-christov model over a stretching sheet through a porous medium in the presence of chemical reaction and suction/injection, *J Porous Media*, 25 (2022) 1.

30 Bataller R C, Effects of heat source/sink, radiation and work done by deformation on flow and heat transfer of a viscoelastic fluid over a stretching sheet, *Comput Math Appl*, 53 (2007) 305.

31 Rashidi M M, Ganesh N V, Hakeem A K A & Ganga B, Buoyancy effect on MHD flow of nanofluid over a stretching sheet in the presence of thermal radiation, *J Mol Liq*, 198 (2014) 234.

32 Reddy M V, Lakshminarayana P & Vajravelu K, Magneto hydrodynamic radiative flow of a Maxwell fluid on an expanding surface with the effects of Dufour and Soret and chemical reaction, *Comput Therm Sci Int J*, 12 (2020) 317.

33 Goud B S, Heat generation/absorption influence on steady stretched permeable surface on MHD flow of a micropolar fluid through a porous medium in the presence of variable suction/injection, *Int J Thermofluids*, 7 (2020) 100044.

34 Ram M S, Shamshuddin M D & Spandana K, Numerical simulation of stagnation point flow in magneto micropolar fluid over a stretchable surface under influence of activation energy and bilateral reaction, *Int Commun Heat Mass Transf*, 129 (2021) 105679.

35 Azam M, Effects of Cattaneo-christov heat flux and nonlinear thermal radiation on MHD Maxwell nanofluid with Arrhenius activation energy, *Case Stud Therm Eng*, 34 (2022) 102048.

36 Khan M I, Alsaedi A, Qayyum S, Hayat T & Khan M I, Entropy generation optimization in flow of Prandtl-eyring nanofluid with binary chemical reaction and Arrhenius activation energy, *Colloids Surf A: Physicochem Eng Asp*, 570 (2019) 117.

37 Ajithkumar M, Lakshminarayana P & Vajravelu K, Peristaltic transport of MHD Ree-eyring fluid through a flexible channel under the influence of activation energy, *Phys Fluids*, 35 (2023) 13.

38 Reddy M V, Lakshminarayana P, Vajravelu K & Sucharitha G, Activation of energy in MHD Casson nanofluid flow through a porous medium in the presence of convective boundary conditions and suction/injection, *Numer Heat Transf Part A: Appl*, 86 (2023) 1069.